

Tunneling Effect in Gapped Phosphorene through Double Barriers

Jilali Seffadi^a, Ilham Redouani^a, Youness Zahidi ^{*b} and Ahmed Jellal^{†a,c}

^aLaboratory of Theoretical Physics, Faculty of Sciences, Chouaib Doukkali University,
PO Box 20, 24000 El Jadida, Morocco

^bMRI Laboratory, Polydisciplinary Faculty, Sultan Moulay Selimane University,
PO Box 145, 25000 Khouribga, Morocco

^cCanadian Quantum Research Center, 204-3002 32 Ave Vernon,
BC V1T 2L7, Canada

Abstract

We study the transport properties of charge carriers in phosphorene with a mass term through double barriers. The solutions of the energy spectrum are obtained and the dependence of the eigenvalues on the barrier potentials and wave vectors in the x -direction is numerically computed. Using the boundary conditions together with the matrix transfer method, we determine transmission and the conductance of our system. These two quantities are analyzed by studying their main characteristics as a function of the physical parameters along the armchair direction. Our results show the highly anisotropic character of phosphorene and the no signature of Klein tunneling at normal incidence contrary to graphene. Moreover, it is found that the transmission and conductance display oscillatory behaviors in terms of the barrier width under suitable conditions.

PACS numbers: 73.22.-f; 73.63.Bd; 72.10.Bg; 72.90.+y

Keywords: Phosphorene, double barriers, energy gap, transmission, conductance.

*y.zahidi@usms.ma

†a.jellal@ucd.ac.ma

1 Introduction

Two dimensional (2D) crystals consisting of single or a few atomic layers has been the focus of instance research currently, due to their fundamental properties and possible applications. Since the first experimental fabrication of graphene [1], a 2D single sheet of carbon honeycomb, the researchers were focused on it because of its unique electronic [2–5], optical [6] and mechanical properties [7, 8]. From then, there is a growing interest in the realization of other (2D) materials. The investigation of analogs of graphene has resulted in the discovery of various single-layer crystals of different elements. Among them, silicon (silicene) [9], germanium (germanene) [10] and a class of materials known as transition-metal dichalcogenides [11]. In recent years, it is showed that such materials serve as test bed for Dirac physics, which arises from the fact that their low-energy quasiparticles obey an effective Dirac-like equation. These quasiparticles lead to a host of unconventional transport properties and distinguishes them from conventional materials obeying the Schrödinger equation.

The black phosphorus is among the most promising 2D materials, which is an allotrope of phosphorus [12–15] and well-known as phosphorene. It has triggered tremendous attention since its first discovery in 2014 [14, 15]. Similarly to graphene, phosphorene can be mechanically exfoliated to obtain samples with a single or few layers. It features an orthorhombic crystal structure, whose individual layers feature a puckered, honeycomb lattice structure and each atom is covalently bonded to three of its neighbor. Phosphorene is a semiconductor and has a high electronic mobility in the range of $1000 \text{ cm}^2 \text{ V}^{-1} \text{ s}^{-1}$ [14], which makes it as a possible candidate for device applications [16, 17]. Its electronic structure [18] shows, in contrast to graphene, an intrinsic band-gap and strong anisotropy, which causes the electrons to behave in one direction like massive Dirac fermions and in the orthogonal direction like non-relativistic Schrödinger electrons [19]. Phosphorene shows a robust direct band gap for all thickness varying from 1.8 eV for single layer to 0.4 eV for bulk samples [14], which depends on the number of layers.

The quantum transport in phosphorene was analyzed under different circumstances. For instance, it was highlighted the anisotropic transport signatures of phosphorene across a NBN junction with different orientations [20]. Additionally, it was shown that for a barrier along the x -direction, the dominant contribution to the transport comes from the quasiparticles, which impinge on the barrier at near-normal incidence provided the applied voltage is close to the bottom of the conduction band, leading to collimated transport of electrons. Recently, it was demonstrated that phosphorene PNP junctions constitute perfect electron waveguides, without any leakage current through the side-walls [21] and at the interfaces of the junction, the omni-directional total reflection takes place, which is not due to an energetically forbidden region but due to pseudo-spin blocking.

Motivated by the results developed in [20, 21], we consider a monolayer phosphorene and study the scattering of charge carriers through double barrier structure with an energy gap in the central region. We solve the eigenvalue equation of the continuum model and then determine the solutions of energy spectrum in different regions. By requiring the continuity of the wave functions at interfaces and using the transfer matrix method, we determine the transmission and the conductance as a function of the physical parameters. Numerically we show that the transmission displays sharp pics inside the transmission gap around some energy values, which are resulted from the quasibound states formed in the double barrier structure. Additionally, our analysis tells us there is no signature of the Klein

tunneling at normal incidence. Moreover, we find that the conductance displays oscillatory behavior as a function of the barrier width.

The present paper is organized as follows. In section 2, we describe our system by setting the appropriate Hamiltonian, which will be used to obtain the eigenvalues and eigenspinors. By applying the boundary conditions at interfaces, we determine the transmission probability and the associated conductance. In section 4, we numerically analyze our results under suitable conditions of the physical parameters. Finally, we conclude our work.

2 Hamiltonian formalism

Recall that phosphorene is a 2D hexagonal lattice that is buckled (or "puckered") due to the hybridization sp^3 . The phosphorus atoms at different sublayers are represented in Figure 1 with sublattices (A, B) at bottom sublayer (pink symbol) and (C, D) at top one (green symbol). This geometry results in two types of bands as shown as in Figure 1(a) where atoms P , connected by bonds parallel to the plane, form upper and lower sublayers, while the bonds connecting atoms P between these two sublayers are oriented by an angle 71.7° out of plane. Figures 1(b,c) present the top and side-view, along the armchair direction, of the lattice structure of monolayer phosphorene. The shaded rectangle indicates the unit cell and the side view highlights the inter-atomic coupling. The hopping parameter t_1 is for the connection along a zigzag direction in the upper or lower sublayer and t_2 is for that between a pair of zigzag chains in the upper and lower sublayers. The parameters t_3 and t_4 are between the nearest-neighbor and next nearest neighbor sites of a pair of zigzag chains in the upper or lower sublayer. The parameter t_5 is between two atoms on upper and lower zigzag chains that are farthest from each other. Figure 1(d) shows the lattice structure of phosphorene, emphasizing the bond lengths and bond angles between the phosphorus atomic sites, with $a_1 = 2.22 \text{ \AA}$ is the distance between nearest neighbour sites in sublattices (A, B) or (C, D) and $a_2 = 2.24 \text{ \AA}$ is that between nearest neighbor sites in sublattices (A, C) or (B, D) . The bond angles are $\alpha_1 = 96.5^\circ$, $\alpha_2 = 101.9^\circ$ and $\beta = 72^\circ$.

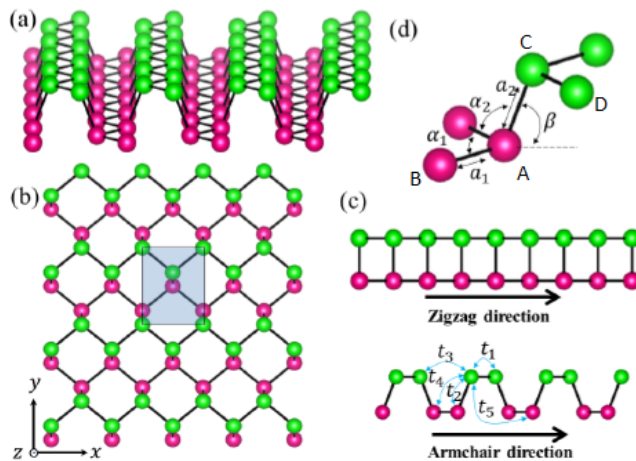


Figure 1 – (a): Bird eye's view of the lattice structure of monolayer phosphorene, where the phosphorus atoms at different sublayers are represented by different colors in each sublayer. (b): 2D lattice of monolayer projected onto the xy -plane. Shaded rectangle indicates the unit cell. (c): The "zigzag" and "armchair" edges with inter-atomic coupling. (d): Lattice structure of monolayer phosphorene systems with the different parameters.

It has been recently shown within the five-hopping parameter approach [22,23] that the continuum approximation is very suited for describing the physics of large phosphorene, yielding very accurate results within its limit of validation. A unitary transformation can be performed to rewrite the monolayer Hamiltonian in a simpler block form. In our case, we consider the block Hamiltonian [22]

$$H^\pm(k) = \begin{pmatrix} t_{AA}(k) \pm t_{AD}(k) & t_{AB}(k) \pm t_{AC}(k) \\ t_{AB}^*(k) \pm t_{AC}^*(k) & t_{AA}(k) \pm t_{AD}(k) \end{pmatrix} \quad (1)$$

where under expansion around the long-wavelength $k = 0$ (Γ point) up to second order, the structure factors become

$$t_{AA}(k) = \delta_{AA} + \eta_{AA}k_y^2 + \gamma_{AA}k_x^2 \quad (2)$$

$$t_{AB}(k) = \delta_{AB} + \eta_{AB}k_y^2 + \gamma_{AB}k_x^2 + i\chi_{AB}k_x \quad (3)$$

$$t_{AC}(k) = \delta_{AC} + \eta_{AC}k_y^2 + \gamma_{AC}k_x^2 + i\chi_{AC}k_x \quad (4)$$

$$t_{AD}(k) = \delta_{AD} + \eta_{AD}k_y^2 + \gamma_{AD} \quad (5)$$

giving rise to the following Hamiltonian

$$H^+(k) = \begin{pmatrix} u_0 + \eta_x k_x^2 + \eta_y k_y^2 & \delta + \gamma_x k_x^2 + \gamma_y k_y^2 + i\chi k_x \\ \delta + \gamma_x k_x^2 + \gamma_y k_y^2 - i\chi k_x & u_0 + \eta_x k_x^2 + \eta_y k_y^2 \end{pmatrix} \quad (6)$$

with the setting

$$u_0 = \delta_{AA} + \delta_{AD}, \quad \delta = \delta_{AB} + \delta_{AC} \quad (7)$$

$$\eta_x = \eta_{AA} + \eta_{AD}, \quad \eta_y = \gamma_{AA} + \gamma_{AD} \quad (8)$$

$$\gamma_x = \eta_{AB} + \eta_{AC}, \quad \gamma_y = \gamma_{AB} + \gamma_{AC} \quad (9)$$

$$\chi = \chi_{AB} + \chi_{AC} \quad (10)$$

$\vec{k} = (k_x, k_y)$ is the wave vector and the coefficient values of the expanded structure factors for both five-hopping models are summarized in Table 1.

	5-hopping		5-hopping		Units
δ_{AA}	0.00	δ_{AB}	-2.85		eV
δ_{AC}	3.61	δ_{AD}	-0.42		eV
η_{AA}	0.00	η_{AB}	3.91		eV \AA^2
η_{AC}	-0.53	η_{AD}	0.58		eV \AA^2
γ_{AA}	0.00	γ_{AB}	4.41		eV \AA^2
γ_{AC}	0.00	γ_{AD}	1.01		eV \AA^2
χ_{AB}	2.41	χ_{AC}	2.84		eV \AA

Table 1 – Structure factor coefficients.

In order to study the scattering of charge carriers in phosphorene, we consider the following double barrier

$$V_j(x) = \begin{cases} V_{1,5} = 0 & \text{if } |x| > d_2, \\ V_2 & \text{if } -d_2 < x < -d_1, \\ V_3 & \text{if } |x| < d_1, \\ V_4 & \text{if } d_1 < x < d_2. \end{cases} \quad (11)$$

where $V_{1,2,3}$ and $d_{1,2,3}$ are positive potential parameters characterizing the double barrier structure shown in Figure 2 with j labeling the five regions.

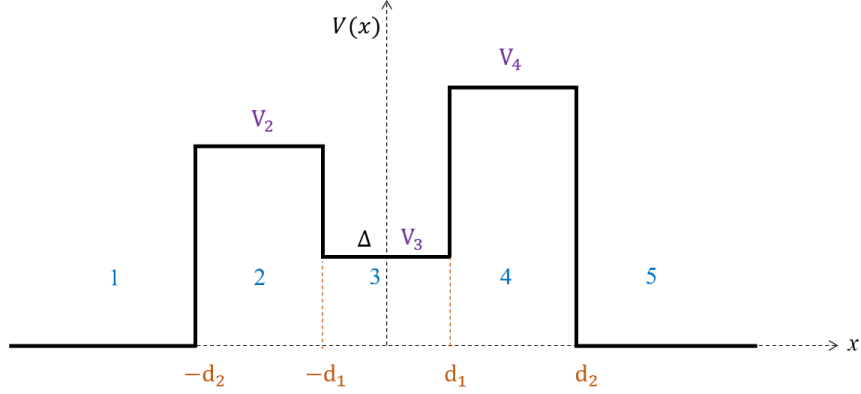


Figure 2 – Schematic profile of the barrier potentials $V(x)$ composed of five regions with three amplitudes (V_2, V_3, V_4) and a gap placed in region 3.

According to the possible profile, the Hamiltonian describing the four regions 1, 2, 4, 5 can be written as

$$H_j(k) = H^+(k) + V_j(x)\mathbb{I}_2 \quad (12)$$

and as for region 3 we have

$$H_3(k) = H^+(k) + V_3(x)\mathbb{I}_2 + \Delta\sigma_z \quad (13)$$

where σ_z is the Pauli matrix and Δ is the involved gap. Then, the dispersion relations can be calculated to end up with the energies in regions $j = (1, 2, 4, 5)$

$$E_j = V_j + u_0 + \eta_x k_{jx}^2 + \eta_y k_y^2 + s_j \sqrt{(\delta + \gamma_x k_{jx}^2 + \gamma_y k_y^2)^2 + (\chi k_{jx})^2} \quad (14)$$

as well as in region 3

$$E_3 = V_3 + u_0 + \eta_x k_{jx}^2 + \eta_y k_y^2 + s_3 \sqrt{(\delta + \gamma_x k_{jx}^2 + \gamma_y k_y^2)^2 + (\chi k_{jx})^2 + \Delta^2} \quad (15)$$

with $s_j = \text{sign}(E - V_j - u_0 - \eta_x k_{jx}^2 - \eta_y k_y^2)$ and $s_3 = \text{sign}(E - V_3 - u_0 - \eta_x k_{jx}^2 - \eta_y k_y^2)$. Note that, the term proportional to k_{jx}^2 in the energy spectrum can be ignored because at low momenta we have $u_0, \delta, k_{jx} \gg k_{jx}^2$ and $k_{jx}^2 < 1$ [20]. The longitudinal wave vectors k_{jx} corresponding to (14) and (15) are given by

$$k_{jx} = \chi^{-1} \sqrt{(E_j - V_j - u_0 - \eta_y k_y^2)^2 - (\delta + \gamma_y k_y^2)^2} \quad (16)$$

$$k_{3x} = \chi^{-1} \sqrt{(E_3 - V_3 - u_0 - \eta_y k_y^2)^2 - (\delta + \gamma_y k_y^2)^2 - (\Delta)^2} \quad (17)$$

We note that the energy spectrum is linear (Dirac like) in k_x but parabolic (Schrödinger like) in k_y . Consequently, the nature of the quasiparticle transport and the effect of a potential barrier depends crucially on the its orientation in the xy -plane. In addition, by increasing the potential height V_3 , the energy bands are shifted upwards also by V_3 , as shown in Figure 3(a). Moreover, we can clearly see the effect of the energy gap, as shown in Figure 3(b), that increase the gap between the valence and conduction bands.

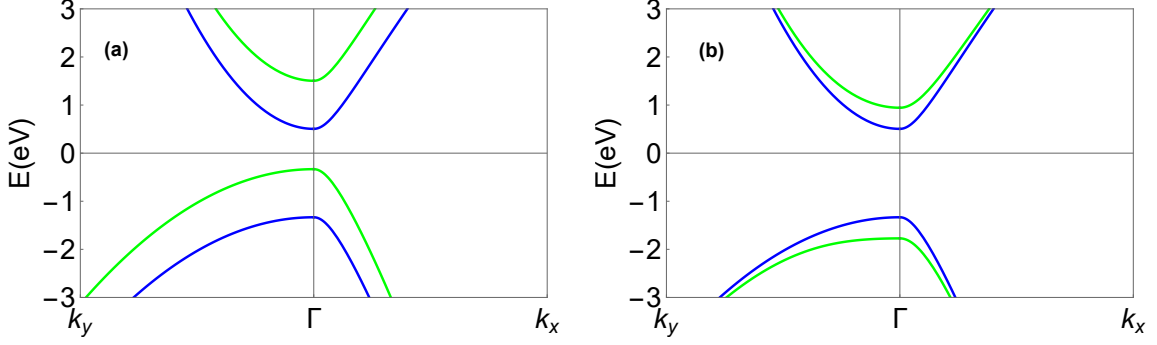


Figure 3 – The energy eigenvalues outside and inside the barrier regions as a function of the wave vector k_y and k_x . (a): $V_3 = 0$ eV and $\Delta = 0$ eV (green lines), $V_3 = 1$ eV and $\Delta = 0$ eV (blue lines). (b): $V_3 = 0$ eV and $\Delta = 1$ eV (green lines), $V_3 = 0$ eV and $\Delta = 0$ eV (blue lines).

The associated eigenspinors to (14) and (15) can be determined by solving the eigenvalue equation $H_j \Phi_j = E_j \Phi_j$. This process yields the solutions in five regions

$$\Phi_1 = \begin{pmatrix} 1 \\ z_1 \end{pmatrix} e^{i(k_{1x}x)} + r \begin{pmatrix} 1 \\ z_1^{-1} \end{pmatrix} e^{i(-k_{1x}x)} \quad (18)$$

$$\Phi_2 = a \begin{pmatrix} 1 \\ z_2 \end{pmatrix} e^{i(k_{2x}x)} + b \begin{pmatrix} 1 \\ z_2^{-1} \end{pmatrix} e^{i(-k_{2x}x)} \quad (19)$$

$$\Phi_3 = c \begin{pmatrix} \sigma \\ \tau z_3 \end{pmatrix} e^{i(k_{3x}x)} + d \begin{pmatrix} \sigma \\ \tau z_3^{-1} \end{pmatrix} e^{i(-k_{3x}x)} \quad (20)$$

$$\Phi_4 = e \begin{pmatrix} 1 \\ z_4 \end{pmatrix} e^{i(k_{4x}x)} + f \begin{pmatrix} 1 \\ z_4^{-1} \end{pmatrix} e^{i(-k_{4x}x)} \quad (21)$$

$$\Phi_5 = t \begin{pmatrix} 1 \\ z_5 \end{pmatrix} e^{i(k_{5x}x)} \quad (22)$$

where we have set $z_j = s_j e^{-i\theta_j}$ with $s_j = \text{sign}(E - V_j - u_0 - \eta_y k_y^2)$ and the involved parameters are given by

$$\theta_j = \arctan \left(\frac{\chi k_{jx}}{\delta + \gamma_y k_y^2} \right) \quad (23)$$

$$\sigma = \sqrt{1 + \frac{s_3 \Delta}{\sqrt{\Delta^2 + (k_{3x})^2}}} \quad (24)$$

$$\tau = \sqrt{1 - \frac{s_3 \Delta}{\sqrt{\Delta^2 + (k_{3x})^2}}} \quad (25)$$

3 Transmission and conductance

Next we will calculate the transmission probability of electrons across the potential barriers in our phosphorene system. In doing so, it is convenient to use the matrix formalism. Using the boundary conditions at interfaces $x = -d_2, -d_1, d_1, d_2$ demanding the eigenspinors continuities

$$\Phi_1(-d_2) = \Phi_2(-d_2), \quad \Phi_2(-d_1) = \Phi_3(-d_1), \quad \Phi_3(d_1) = \Phi_4(d_1), \quad \Phi_4(d_2) = \Phi_5(d_2) \quad (26)$$

which can be mapped as

$$M_1[-d_2] \begin{pmatrix} 1 \\ r \end{pmatrix} = M_2[-d_2] \begin{pmatrix} a \\ b \end{pmatrix} \quad (27)$$

$$M_2[-d_1] \begin{pmatrix} a \\ b \end{pmatrix} = M_3[-d_1] \begin{pmatrix} c \\ d \end{pmatrix} \quad (28)$$

$$M_3[d_1] \begin{pmatrix} c \\ d \end{pmatrix} = M_4[d_1] \begin{pmatrix} e \\ f \end{pmatrix} \quad (29)$$

$$M_4[d_2] \begin{pmatrix} e \\ f \end{pmatrix} = M_5[d_2] \begin{pmatrix} t \\ 0 \end{pmatrix} \quad (30)$$

and then after a simple manipulation we get

$$\begin{pmatrix} 1 \\ r \end{pmatrix} = M \begin{pmatrix} t \\ 0 \end{pmatrix} \quad (31)$$

where the introduced transfer matrix is given by

$$M = M_1^{-1}[-d_2] M_2[-d_2] M_2^{-1}[-d_1] M_3[-d_1] M_3^{-1}[d_1] M_4[d_1] M_4^{-1}[d_2] M_5[d_2] \quad (32)$$

$$= \begin{pmatrix} M_{11} & M_{12} \\ M_{21} & M_{22} \end{pmatrix} \quad (33)$$

Since the wave vector incident and transmitted waves is the same, therefore, the transmission probability can be obtained as

$$T = |t|^2 = \frac{1}{|M_{11}|^2} \quad (34)$$

where t is given by

$$t = \frac{16\tau\sigma s_1 s_2 s_3 s_4 \sin\theta_1 \sin\theta_2 \sin\theta_3 \sin\theta_4 e^{i(d_2(-2k_{1x}+k_{2x}+k_{4x})+d_1(k_{2x}+2k_{3x}+k_{4x}))}}{e^{4id_1 k_{3x}} A_1 A_2 + B_1 B_2} \quad (35)$$

and the parameters are

$$A_1 = (z_1 - z_4^{-1})(z_4\sigma - z_3\tau)e^{2id_1 k_{4x}} + (z_1 - z_4)(z_4^{-1}\sigma - z_3\tau)e^{2id_2 k_{4x}} \quad (36)$$

$$A_2 = (z_1^{-1} - z_2^{-1})(z_2\sigma - z_3^{-1}\tau)e^{2id_2 k_{2x}} + (z_1^{-1} - z_2)(z_2^{-1}\sigma - z_3^{-1}\tau)e^{2id_1 k_{2x}} \quad (37)$$

$$B_1 = (z_1 - z_4)(z_4^{-1}\sigma - z_3^{-1}\tau)e^{2id_2 k_{4x}} + (z_1 - z_4^{-1})(z_4\sigma - z_3\tau)e^{2id_1 k_{4x}} \quad (38)$$

$$B_2 = (z_1^{-1} - z_2^{-1})(z_2\sigma - z_3\tau)e^{2id_2 k_{2x}} + (z_1^{-1} - z_2)(z_2^{-1}\sigma - z_3\tau)e^{2id_1 k_{2x}}. \quad (39)$$

To complete our study, we investigate an important physical quantity relevant to double barrier structure in phosphorene that is the conductance. Then, using the Landauer-Buttiker formula [20] and obtained transmission probability we get

$$G = G_0 \int_{-k_y^{\max}}^{k_y^{\max}} \frac{dk_y}{2\pi} T \quad (40)$$

where $G_0 = \frac{e^2 L_y}{h}$ is the unit conductance, L_y is the width of the sample in the y -direction and k_y^{\max} denotes the maximum transverse momenta. In next section, we will study numerically these two quantities. This will help us understand the effect of various physical parameters on the transmission and the conductance related to our double barrier structure.

4 Results and discussions

Figure 4 shows the transmission probability as a function of the wave vector k_y for different values of barrier width d and incident energy E . The barrier heights are fixed at $V_2 = V_4 = 12$ eV, $V_3 = 4$ eV, and the gap $\Delta = 0$ eV. T is plotted for $d = 3$ Å (red line), 15 Å (blue line), 20 Å (green line), 25 Å (black line) in Figure 4(a) for $E = 6$ (red line), 7 (blue line) and 8 eV (green line) in Figure 4(b). We observe that the transmission is bilaterally symmetrical with respect to the normal incidence, i.e. $k_y = 0$, and exhibits a behavior similar to that observed for Dirac particle in graphene [24–26]. It is important to note that in the case of graphene in the absence of a magnetic field, the perfect transmission situation appears very clearly in the case $k_y = 0$ (signature of Klein tunneling), which is not the case in our system made of phosphorene. As shown in Figure 4(a), the transmission through thin barriers is negligible compared to that for large d , such behavior is similar to that seen for the transmission through a single barrier in monolayer phosphorene [20]. From Figure 4(b), we notice that the transmission vanishes for specific values that increase by increasing E . Note that when k_y exceed a critical value the transmission probability goes to zero (the transmission is blocked by the barrier) due to the evanescent nature of the states in the barrier. There exist several line-shaped peaks in the forbidden transmission region that are consequences of resonant transmission through the double barrier. The number of resonant peaks changes with the change of the energy value as can be seen in Figure 4(b).

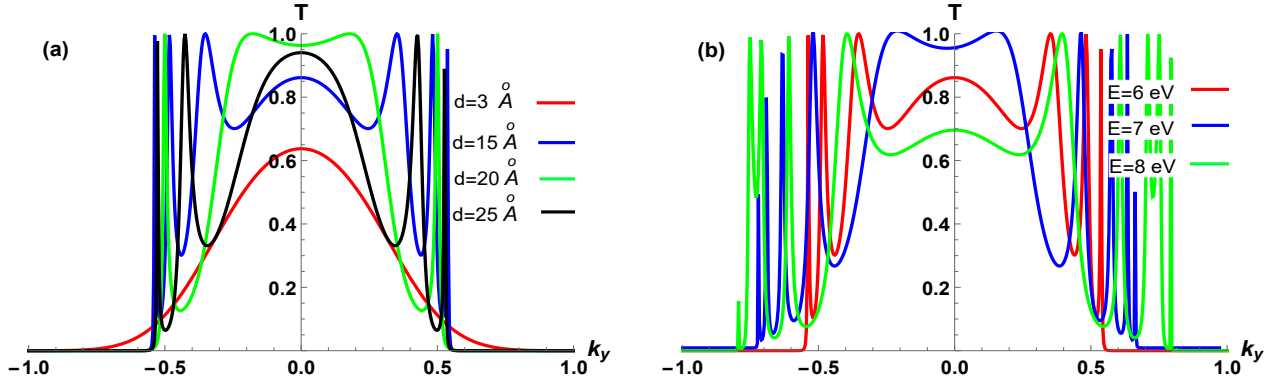


Figure 4 – Transmission probability T as a function of k_y , with $V_2 = V_4 = 12$ eV, $V_3 = 4$ eV, $\Delta = 0$ eV and $d_2 = 2d_1 = d$ for different values of d and E . (a) : $d = 3$ Å (red line), $d = 15$ Å (blue line), $d = 20$ Å (green line), $d = 25$ Å (black line) and $E = 6$ eV. (b) : $E = 6$ eV (red line), $E = 7$ eV (blue line), $E = 8$ eV (green line) and $d = 25$ Å.

In Figure 5, we present the transmission probability as a function of the transverse wave vector k_y and the energy E for four configurations of the double barrier. It is clearly seen that there are different energy zones characterizing the transmission. Indeed, Figure 5(a) corresponds to the case $V_2 < V_3 < V_4$ and shows seven energy zones. At normal incidence, we observe that the first, third and fifth zones are bounded by the energy intervals $0 < E < V_2 + u_0 - \delta$, $V_2 + u_0 + \delta < E < V_3 + u_0 - \delta$ and $V_3 + u_0 + \delta < E < V_4 + u_0 - \delta$, respectively, which contains oscillations (resonances) in the transmission. While the transmission is zero in the second, fourth and sixth zones $V_i + u_0 - \delta < E < V_i + u_0 + \delta$ with $i = 2, 3$ and 4, respectively. It is important to note that the transmission displays sharp peaks inside the transmission gap around the point $E = V_2 + u_0$ and $E = V_4 + u_0$, but they are absent around the energy point $E = V_3 + u_0$. Finally, the seventh zone $E > V_4 + u_0 + \delta$ contains the usual

high energy barrier oscillations and asymptotically goes to unity at high energy. It is important to note that, the transmission exhibit the same behavior for both cases $V_2 < V_4 < V_3$ and $V_3 < V_2 < V_4$ as shown in Figure 5(b,c). From Figure 5(d) for $V_2 = V_4 \neq V_3$, we observe that there are only five energy zones where in the first ($0 < E < V_2 + u_0 - \delta$) and third ($V_2 + u_0 - \delta < E < V_4 + u_0 + \delta$) zones, the transmission exhibits an oscillatory behavior as a function of the incident energy. Moreover, the transmission displays sharp peaks inside the transmission gap around the point $E = V_2 + u_0 = V_4 + u_0$, that are absent around $E = V_3 + u_0$. These peaks can be attributed to the quasi-bound states formed in the double barrier structure in similar way to that obtained for graphene [27].

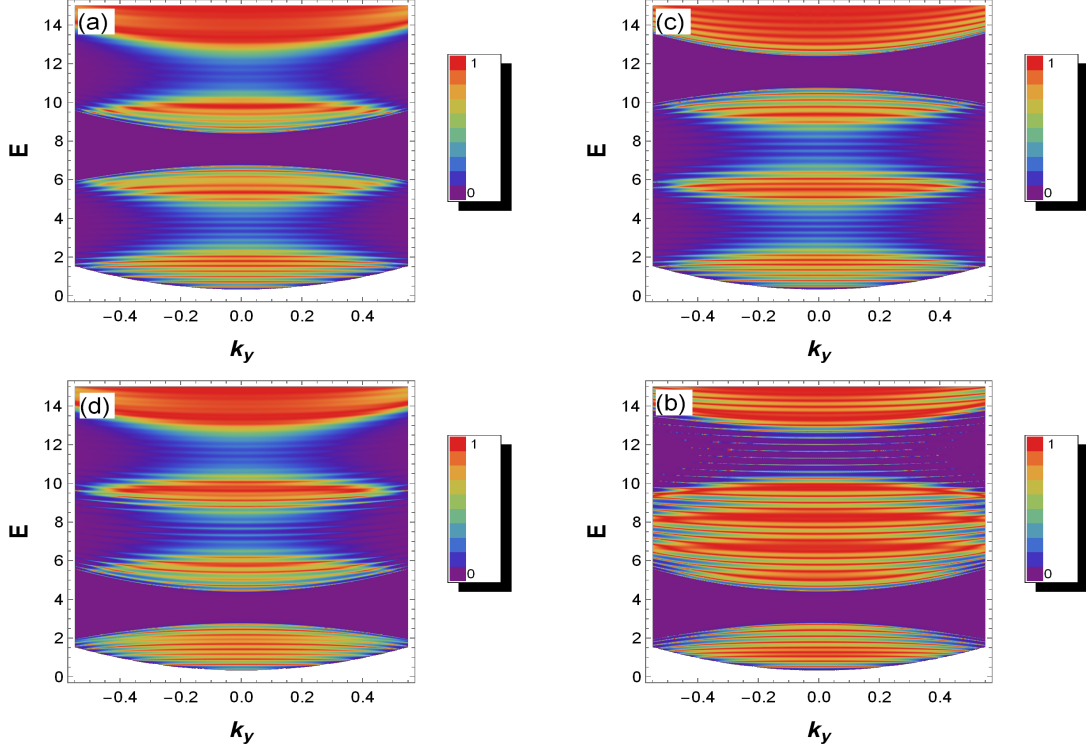


Figure 5 – Density plot of transmission probability T as a function of the transverse wave vector k_y and energy E , with $d_1 = 20 \text{ \AA}$, $d_2 = 30.3 \text{ \AA}$ and $\Delta = 0 \text{ eV}$, for different barrier structures. (a): $V_2 = 4 \text{ eV}$, $V_3 = 8 \text{ eV}$ and $V_4 = 12 \text{ eV}$. (b): $V_2 = V_4 = 12 \text{ eV}$ and $V_3 = 4 \text{ eV}$. (c): $V_2 = 4 \text{ eV}$, $V_3 = 12 \text{ eV}$ and $V_4 = 8 \text{ eV}$. (d): $V_2 = 8 \text{ eV}$, $V_3 = 4 \text{ eV}$ and $V_4 = 12 \text{ eV}$.

We now investigate the effect of the introduced gap Δ on the transmission probability T in Figure 6, which has been performed by fixing the parameters $d_1 = 20 \text{ \AA}$, $d_2 = 30.3 \text{ \AA}$ and $k_y = 0$ for different barrier structures as in Figure 5. We observe that for $\Delta = 0$, T exhibits sharp peaks around $E = V_2 + u_0$ and $E = V_4 + u_0$, but they are absent around $E = V_3 + u_0$, which confirm what we found in Figure 5. It is clearly seen that as long as Δ the transmission gap around $E = V_3 + u_0$ increases in all cases and for large Δ , the transmission oscillation starts to decrease until vanishing.

It is worth while to investigate the conductance as a function of the incident energy together with transmission in Figure 7. To analyze the conductance behavior we distinguish five zones such that in the first zone ($E < V_3 + u_0 - \delta$), the resonances in the transmission correspond to peaks in the conductance. The second zone ($V_3 + u_0 - \delta < E < V_3 + u_0 + \delta$) shows a window where T and G/G_0 are zero. In the third zone ($V_3 + u_0 + \delta < E < V_4 + u_0 - \delta$), the peaks in conductance have shoulders due to the presence of resonances in the transmission. We notice that the number of peaks is the

same for the transmission and the conductance. The fourth ($V_4 + u_0 - \delta < E < V_4 + u_0 + \delta$) presents a bowl where T and G/G_0 are mostly zero but contains resonances peaks. The fifth zone ($V_1 < E_1$) contains oscillations, the transmission converges to unity at high energies and conductance researches a maximum value.

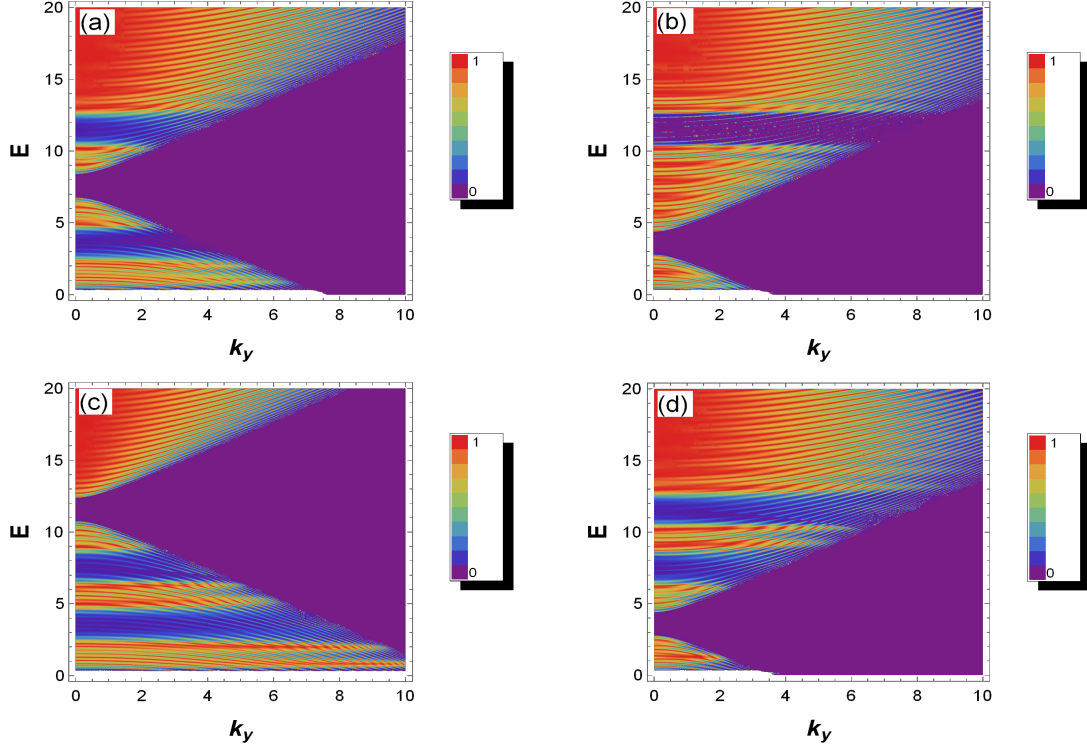


Figure 6 – Density plot of transmission probability T as a function of energy gap Δ and incident energy E with $d_1 = 20 \text{ \AA}$, $d_2 = 30.3 \text{ \AA}$ and $k_y = 0 \text{ \AA}^{-1}$ for different barrier structures. (a): $V_2 = 4 \text{ eV}$, $V_3 = 8 \text{ eV}$ and $V_4 = 12 \text{ eV}$. (b): $V_2 = V_4 = 12 \text{ eV}$ and $V_3 = 4 \text{ eV}$. (c): $V_2 = 4 \text{ eV}$, $V_3 = 12 \text{ eV}$ and $V_4 = 8 \text{ eV}$. (d): $V_2 = 8 \text{ eV}$, $V_3 = 4 \text{ eV}$ and $V_4 = 12 \text{ eV}$.

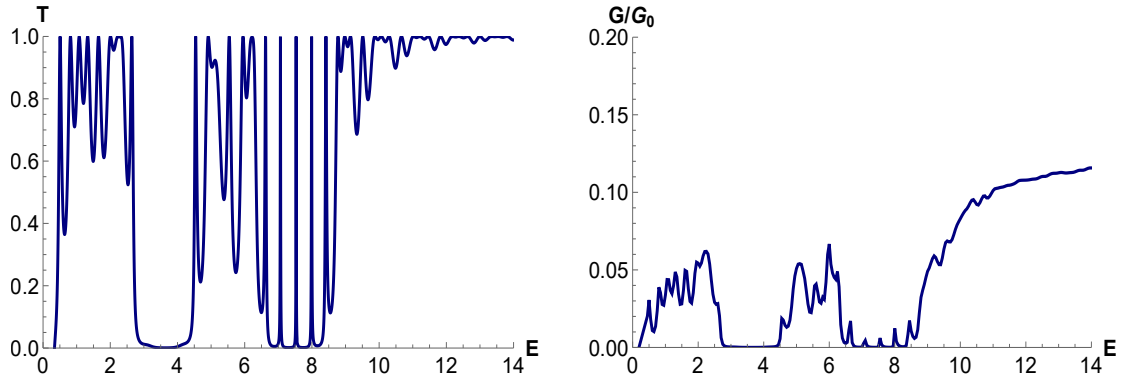


Figure 7 – Transmission probability and conductance as a function of the incident energy E for $d_2 = 2d_1 = d = 12 \text{ \AA}$, $\Delta = 0$, $V_2 = V_4 = 8 \text{ eV}$, $V_3 = 4 \text{ eV}$ and $k_y = 0$.

Figure (8) is intended to see the influence of the barrier width d for different values of the central potential V_3 . It is clearly seen that the transmission T and conductance G/G_0 are either a decaying or an oscillatory depending on the value of V_3 . For the range $E < V_4 + u_0 < V_3 + u_0$, T and G/G_0 display oscillatory behavior with the increase of d in similar way to that of massless Dirac like electrons as

seen in graphene [27]. However in contrast to graphene, T and G/G_0 show a sharp decay as a function of d when $E < V_3 + u_0 < V_4 + u_0$. For $V_3 + u_0 < E < V_4 + u_0$, T and G/G_0 show an oscillatory behavior similar to single and multiple barrier structure in monolayer phosphorene [20].

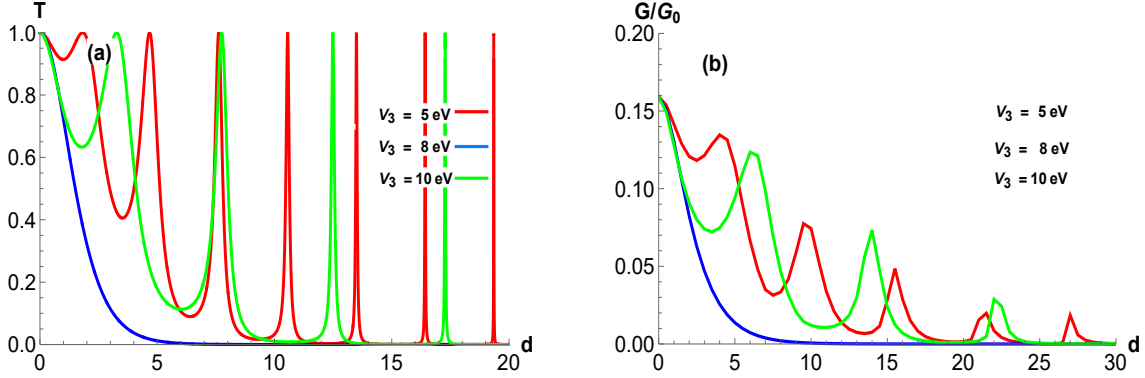


Figure 8 – The transmission probability T and conductance G/G_0 as a function of the barrier width d with $d_1 = d/2$, $d_2 = d$ for $\Delta = 0$ eV, $E = 7.5$ eV and $k_y = 0$. $V_2 = V_4 = 8$ eV, $V_3 = 5$ eV (red solid line), $V = 8$ eV (blue solid line), $V = 10$ eV (green solid line).

5 Conclusion

We have investigated the transport properties of charge carriers transmitted through monolayer phosphorene with double barriers. We have started by formulating the Hamiltonian model describing our system and getting the associated energy bands. We have shown that the anisotropic properties arise from the difference between $\Gamma - X$ and $\Gamma - Y$ dispersions corresponding to the armchair and zigzag directions, respectively. Subsequently, by using the transfer matrix method, we have calculated the transmission as well as the conductance in terms of the physical parameters.

Our numerical analysis showed that the transmission displays sharp pics inside the transmission gap around $E = V_4 + u_0$ and $E = V_2 + u_0$, which are absent around $E = V_3 + u_0$. These peaks can be attributed to the quasi-bound states formed in the double barrier structure. This behavior was observed in monolayer graphene with double barrier structure. Moreover, we have found that the transmission is bilaterally symmetrical with respect to the normal incidence k_y and there is no signature of the Klein tunneling contrary to graphene. It was argued with the increase of k_y the transmission vanishes for some specific values depending on the incident energy. We have observed that the transmission through thin barriers is negligible compared to that in single barrier for large width d . It was shown that when k_y exceed a critical value the transmission is blocked by the barrier, which is due to the evanescent nature of the states in the barrier. We have seen that many line-shaped peaks appeared in the forbidden transmission region whose number changes with the change of energy that are the consequences of resonant transmission through the double barrier.

Finally, we have shown that the transmission and the conductance display oscillatory behavior as a function of the barrier width d for both cases $E < V_4 + u_0 < V_3 + u_0$ and $V_3 + u_0 < E < V_4 + u_0$, but sharp decay for $E < V_3 + u_0 < V_4 + u_0$ similar to that obtained for single barrier in phosphorene. It was found that the conductance as a function of the incident energy presents a behavior similar to the transmission one. It was argued that for $E < V_3 + u_0 - \delta$ the resonances in transmission correspond

to peaks in conductance. Moreover, around $E = V_3 + u_0$ and $E = V_4 + u_0$, we have found that the conductance is zero, while the peaks in the conductance around $E = V_4 + u_0$ are due to the presence of resonances in the transmission probability.

References

- [1] K. S. Novoselov, A. K. Geim, S. V. Morozov, D.-e. Jiang, Y. Zhang, S. V. Dubonos, I. V. Grigorieva, A. A. Firsov, *Science* 306 (2004) 666.
- [2] A. C. Neto, F. Guinea, N. M. Peres, K. S. Novoselov, A. K. Geim, *Reviews of Modern Physics* 81 (2009) 109.
- [3] L. E. F. Torres, S. Roche, J.-C. Charlier, *Introduction to graphene-based nanomaterials: from electronic structure to quantum transport* (Cambridge University Press, 2014).
- [4] M. Katsnelson, K. Novoselov, A. Geim, *Nature physics* 2 (2006) 620.
- [5] K. Novoselov, S. Morozov, T. Mohinddin, L. Ponomarenko, D. Elias, R. Yang, I. Barbolina, P. Blake, T. Booth, D. Jiang, J. Giesbers, E. W. Hill, A. K. Geim, *Physica Status Solidi (b)* 244 (2007) 4106.
- [6] J. Qiao, X. Kong, Z.-X. Hu, F. Yang, W. Ji, *Nature Communications* 5 (2014) 1.
- [7] D. G. Papageorgiou, I. A. Kinloch, R. J. Young, *Progress in Materials Science* 90 (2017) 75.
- [8] I. Ovid'Ko, *Reviews on Advanced Materials Science* 34 (2013) 1.
- [9] P. De Padova, C. Ottaviani, C. Quaresima, B. Olivieri, P. Imperatori, E. Salomon, T. Angot, L. Quagliano, C. Romano, A. Vona, *2D Materials* 1 (2014) 021003.
- [10] M. Dávila, L. Xian, S. Cahangirov, A. Rubio, G. Le Lay, *New Journal of Physics* 16 (2014) 095002.
- [11] B. Radisavljevic, A. Radenovic, J. Brivio, V. Giacometti, A. Kis, *Nature Nanotechnology* 6 (2011) 147.
- [12] L. Li, Y. Yu, G. J. Ye, Q. Ge, X. Ou, H. Wu, D. Feng, X. H. Chen, Y. Zhang, *Nature Nanotechnology* 9 (2014) 372.
- [13] A. Rodin, A. Carvalho, A. C. Neto, *Physical Review Letters* 112 (2014) 176801.
- [14] S. P. Koenig, R. A. Doganov, H. Schmidt, A. Castro Neto, B. Özyilmaz, *Applied Physics Letters* 104 (2014) 103106.
- [15] H. Liu, A. T. Neal, Z. Zhu, Z. Luo, X. Xu, D. Tománek, P. D. Ye, *ACS nano* 8 (2014) 4033.
- [16] D. K. Sang, H. Wang, Z. Guo, N. Xie, H. Zhang, *Advanced Functional Materials* 29 (2019) 1903419.
- [17] L. Li, Y. Yu, G. J. Ye, Q. Ge, X. Ou, H. Wu, D. Feng, X. H. Chen, Y. Zhang, *Nature Nanotechnology* 9 (2014) 372.

- [18] S. Fukuoka, T. Taen, T. Osada, *Journal of the Physical Society of Japan* 84 (2015) 121004.
- [19] L. Li, B. Partoens, F. Peeters, *Physical Review B* 97 (2018) 155424.
- [20] S. De Sarkar, A. Agarwal, K. Sengupta, *Journal of Physics: Condensed Matter* 29 (2017) 285601.
- [21] Y. Betancur-Ocampo, E. Paredes-Rocha, T.s Stegmann, *Journal of Applied Physics* 128 (2020) 114303.
- [22] J. Pereira Jr, M. Katsnelson, *Physical Review B* 92 (2015) 075437.
- [23] D. De Sousa, L. De Castro, D. Da Costa, J. M. Pereira Jr, *Physical Review B* 94 (2016) 235415.
- [24] L. Liu, Y.-X. Li, J.-J. Liu, *Physics Letters A* 376 (2012) 3342.
- [25] J.-H. Yuan, J.-J. Zhang, Q.-J. Zeng, J.-P. Zhang, Z. Cheng, , *Physica B* 406 (2011) 4214.
- [26] Y. Zahidi, I. Redouani, A. Jellal, *Physica E* 81 (2016) 259.
- [27] A. Jellal, I. Redouani, Y. Zahidi, H. Bahlouli, *Physica E* 58 (2014) 30.